

Search for 14.4 keV solar axions from M1 transition of ^{57}Fe with CUORE crystals

F. Alessandria,¹ R. Ardito,² D. R. Artusa,^{3,4} F. T. Avignone III,³ O. Azzolini,⁵ M. Balata,⁴ T. I. Banks,^{4,6,7} G. Bari,⁸ J. Beeman,⁹ F. Bellini,^{10,11} A. Bersani,¹² M. Biassoni,^{13,14} T. Bloxham,⁷ C. Brofferio,^{13,14} C. Bucci,⁴ X. Z. Cai,¹⁵ L. Canonica,⁴ S. Capelli,^{13,14} L. Carbone,¹⁴ L. Cardani,^{10,11} M. Carrettoni,^{13,14} N. Casali,⁴ N. Chott,³ M. Clemenza,^{13,14} C. Cosmelli,^{10,11} O. Cremonesi,^{*14} R. J. Creswick,³ I. Dafinei,¹¹ A. Dally,¹⁶ V. Datskov,¹⁴ A. De Biasi,⁵ M. P. Decowski,^{#6,7} M. M. Deninno,⁸ S. Di Domizio,^{12,17} M. L. di Vacri,⁴ L. Ejzak,¹⁶ R. Faccini,^{10,11} D. Q. Fang,¹⁵ H. A. Farach,³ E. Ferri,^{13,14} F. Ferroni,^{10,11} E. Fiorini,^{13,14} M. A. Franceschi,¹⁸ S. J. Freedman,^{†6,7} B. K. Fujikawa,⁷ A. Giachero,¹⁴ L. Gironi,^{13,14} A. Giuliani,¹⁹ J. Goett,⁴ P. Gorla,²⁰ C. Gotti,^{13,14} E. Guardincerri,^{‡4,7} T. D. Gutierrez,²¹ E. E. Haller,^{9,22} K. Han,⁷ K. M. Heeger,¹⁶ H. Z. Huang,²³ R. Kadel,²⁴ K. Kazkaz,²⁵ G. Keppel,⁵ L. Kogler,^{§6,7} Yu. G. Kolomensky,^{6,24} D. Lenz,¹⁶ Y. L. Li,¹⁵ C. Ligi,¹⁸ X. Liu,²³ Y. G. Ma,¹⁵ C. Maiano,^{13,14} M. Maino,^{13,14} M. Martinez,²⁶ R. H. Maruyama,¹⁶ N. Moggi,⁸ S. Morganti,¹¹ T. Napolitano,¹⁸ S. Newman,^{3,4} S. Nisi,⁴ C. Nones,²⁷ E. B. Norman,^{25,28} A. Nucciotti,^{13,14} F. Orio,¹¹ D. Orlandi,⁴ J. L. Ouellet,^{6,7} M. Pallavicini,^{12,17} V. Palmieri,⁵ L. Pattavina,¹⁴ M. Pavan,^{13,14} M. Pedretti,²⁵ G. Pessina,¹⁴ S. Pirro,¹⁴ E. Previtali,¹⁴ V. Rampazzo,⁵ F. Rimondi,^{†8,29} C. Rosenfeld,³ C. Rusconi,¹⁴ S. Sangiorgio,²⁵ N. D. Scielzo,²⁵ M. Sisti,^{13,14} A. R. Smith,³⁰ L. Taffarello,³¹ M. Tenconi,¹⁹ W. D. Tian,¹⁵ C. Tomei,¹¹ S. Trentalange,²³ G. Ventura,^{32,33} M. Vignati,¹¹ B. S. Wang,^{25,28} H. W. Wang,¹⁵ C. A. Whitten Jr.,^{†23} T. Wise,¹⁶ A. Woodcraft,³⁴ L. Zanotti,^{13,14} C. Zarra,⁴ B. X. Zhu,²³ S. Zucchelli^{8,29} (The CUORE Collaboration)

¹INFN - Sezione di Milano, Milano I-20133 - Italy

²Dipartimento di Ingegneria Strutturale, Politecnico di Milano, Milano I-20133 - Italy

³Department of Physics and Astronomy, University of South Carolina, Columbia, SC 29208 - USA

⁴INFN - Laboratori Nazionali del Gran Sasso, Assergi (L'Aquila) I-67010 - Italy

⁵INFN - Laboratori Nazionali di Legnaro, Legnaro (Padova) I-35020 - Italy

⁶Department of Physics, University of California, Berkeley, CA 94720 - USA

⁷Nuclear Science Division, Lawrence Berkeley National Laboratory, Berkeley, CA 94720 - USA

⁸INFN - Sezione di Bologna, Bologna I-40127 - Italy

⁹Materials Science Division, Lawrence Berkeley National Laboratory, Berkeley, CA 94720 - USA

¹⁰Dipartimento di Fisica, Sapienza Università di Roma, Roma I-00185 - Italy

*Corresponding author: cuore-spokesperson@lngs.infn.it

#Presently at: Nikhef, 1098 XG Amsterdam - The Netherlands

†deceased

‡Presently at: Los Alamos National Laboratory, Los Alamos, NM 87545 - USA

§Presently at: Sandia National Laboratories, Livermore, CA 94551 - USA

†deceased

- ¹¹INFN - Sezione di Roma, Roma I-00185 - Italy
- ¹²INFN - Sezione di Genova, Genova I-16146 - Italy
- ¹³Dipartimento di Fisica, Università di Milano-Bicocca, Milano I-20126 - Italy
- ¹⁴INFN - Sezione di Milano Bicocca, Milano I-20126 - Italy
- ¹⁵Shanghai Institute of Applied Physics (Chinese Academy of Sciences), Shanghai 201800 - China
- ¹⁶Department of Physics, University of Wisconsin, Madison, WI 53706 - USA
- ¹⁷Dipartimento di Fisica, Università di Genova, Genova I-16146 - Italy
- ¹⁸INFN - Laboratori Nazionali di Frascati, Frascati (Roma) I-00044 - Italy
- ¹⁹Centre de Spectrométrie Nucléaire et de Spectrométrie de Masse, 91405 Orsay Campus - France
- ²⁰INFN - Sezione di Roma Tor Vergata, Roma I-00133 - Italy
- ²¹Physics Department, California Polytechnic State University, San Luis Obispo, CA 93407 - USA
- ²²Department of Materials Science and Engineering, University of California, Berkeley, CA 94720 - USA
- ²³Department of Physics and Astronomy, University of California, Los Angeles, CA 90095 - USA
- ²⁴Physics Division, Lawrence Berkeley National Laboratory, Berkeley, CA 94720 - USA
- ²⁵Lawrence Livermore National Laboratory, Livermore, CA 94550 - USA
- ²⁶Laboratorio de Física Nuclear y Astroparticulas, Universidad de Zaragoza, Zaragoza 50009 - Spain
- ²⁷Service de Physique des Particules, CEA/Saclay, 91191 Gif-sur-Yvette - France
- ²⁸Department of Nuclear Engineering, University of California, Berkeley, CA 94720 - USA
- ²⁹Dipartimento di Fisica, Università di Bologna, Bologna I-40127 - Italy
- ³⁰EH&S Division, Lawrence Berkeley National Laboratory, Berkeley, CA 94720 - USA
- ³¹INFN - Sezione di Padova, Padova I-35131 - Italy
- ³²Dipartimento di Fisica, Università di Firenze, Firenze I-50125 - Italy
- ³³INFN - Sezione di Firenze, Firenze I-50125 - Italy
- ³⁴SUPA, Institute for Astronomy, University of Edinburgh, Blackford Hill, Edinburgh EH9 3HJ - UK

Abstract. We report the results of a search for axions from the 14.4 keV M1 transition from ^{57}Fe in the core of the sun using the axio-electric effect in TeO_2 bolometers. The detectors are $5 \times 5 \times 5 \text{ cm}^3$ crystals operated at about 10 mK in a facility used to test bolometers for the CUORE experiment at the Laboratori Nazionali del Gran Sasso in Italy. An analysis of 43.65 kg·d of data was made using a newly developed low energy trigger which was optimized to reduce the energy threshold of the detector. An upper limit of $0.58 \text{ c} \cdot \text{kg}^{-1} \cdot \text{d}^{-1}$ is established at 95% C.L., which translates into lower bounds $f_A \geq 3.12 \times 10^5 \text{ GeV}$ 95% C.L. (DFSZ model) and $f_A \geq 2.41 \times 10^4 \text{ GeV}$ 95% C.L. (KSVZ model) on the Peccei-Quinn symmetry-breaking scale, for a value of $S = 0.5$ of the flavor-singlet axial vector matrix element. These bounds can be expressed in terms of axion masses as $m_A \leq 19.2 \text{ eV}$ and $m_A \leq 250 \text{ eV}$ at 95% C.L. in the DFSZ and KSVZ models respectively. Bounds are given also for the interval $0.35 \leq S \leq 0.55$.

Contents

1	Introduction	1
2	Axion-nucleon coupling: axion emission from ^{57}Fe nuclei in the Sun	2
3	Axion interaction with matter: the axio-electric effect	3
4	Experiment	6
5	Results	8
6	Limits on the axion-relevant parameters	8
7	Summary and Conclusions	10
8	Acknowledgments	11

1 Introduction

Quantum chromodynamics or QCD, largely accepted as the best theory describing strong interactions, contains one curious blemish known as “the strong CP problem”. QCD predicts a large neutron electric dipole moment, of the order $|d_n| \approx 10^{-16}\text{e}\cdot\text{cm}$, whereas the experimental bound is $|d_n| \leq 2.9 \times 10^{-26}\text{e}\cdot\text{cm}$ [1]. This fact puts an unnaturally small upper limit ($< 10^{-10}$) to the θ_{QCD} parameter, the strength of the CP violating term present in the QCD. In order to explain this small value Roberto Peccei and Helen Quinn proposed [2] that the QCD Lagrangian possessed an additional global U(1) symmetry which modified the CP-violating term to:

$$\mathcal{L}_\theta = (\theta_{QCD} - \frac{a}{f_A}) \frac{g_s^2}{32\pi^2} G_a^{\mu\nu} \tilde{G}_{a\mu\nu}, \quad (1.1)$$

where g_s is the strong coupling constant, $G_a^{\mu\nu}$ the gluon field, $\tilde{G}_{a\mu\nu}$ is its dual which violates CP symmetry, a is a new pseudoscalar field, and f_A is the Peccei-Quinn symmetry-breaking scale. Non-perturbative effects induce a potential for the field a that has a minimum at $a = f_A\theta_{QCD}$ which causes the spontaneous breaking of the global U(1) symmetry. Later Weinberg [3] and Wilczek [4], independently pointed out the properties of the Goldstone boson (the axion) resulting from the breaking of the U(1) symmetry.

The axion has a long history, with many theoretical and experimental papers published since the two seminal papers by Weinberg and Wilczek in 1978. Rather than attempt to review the subject, we refer the reader to comprehensive reviews by Raffelt [5], Hagmann et. al [6], and Kim [7], and the many references therein. We will just recall here that the “standard” Peccei-Quinn axion with a symmetry-breaking scale of the order of the electro-weak scale is ruled out by experiments. However, other models of “invisible” axions which break the symmetry at much higher energies are still viable. The possibility that the axion might be most or part of the dark-matter has reinforced even further the interest for this field [8].

The purpose of the present work is to study the interaction of axions produced in the Sun with a terrestrial detector consisting of an array of TeO_2 bolometers operated underground

and described in Section 4. The axion production mechanism is a competing branch of the M1 nuclear ground-state transition in ^{57}Fe in the solar core. This first excited state at 14.4-keV is populated by thermal excitation as discussed in Section 2. The detection mechanism relies on the axio-electric effect occurring in our TeO_2 detectors, which is the analogue of a photo-electric effect with the absorption of an axion instead of a photon.

In this paper we will initially perform a totally model independent study, assuming that the coupling constants related both to the detection and production mechanisms are unconstrained free parameters. We will then focus on the non-hadronic axions that couple to gluons, electrons, and photons described in the model by Dine, Fischler, Srednicki, and Zhitnitski (DFSZ)[9]. In DFSZ or Grand-Unified Theory (GUT) model, axions couple to photons, gluons, and leptons at the tree level: this model is therefore quite appropriate for our experimental approach, which uses the coupling to electrons as a basic detection method. We will also consider another model by Kim and Shifman, Vainstein, and Zakharov [10], the KSVZ or hadronic model, in which no coupling to leptons at the tree level occurs, but a weak radiatively induced coupling to electrons is possible due to axion's interaction with photons.

In both the DFSZ and KSVZ models, the mass of the axion, m_A , is directly related to the Peccei-Quinn symmetry-breaking scale, f_A , through the relation (1.2) where $m_\pi = 135$ MeV is the mass of the pion, $f_\pi \approx 92$ MeV the pion decay constant, while for the mass ratios $z = m_u/m_d = 0.56$ and $w = m_u/m_s = 0.029$, m_u , m_d and m_s are the masses of the up, the down and the strange quark respectively[11]:

$$m_A = \left(\frac{z}{(1+z+w)(1+z)} \right)^{\frac{1}{2}} \frac{f_\pi m_\pi}{f_A} = 6 \text{ [eV]} \left(\frac{10^6}{f_A \text{ [GeV]}} \right). \quad (1.2)$$

2 Axion-nucleon coupling: axion emission from ^{57}Fe nuclei in the Sun

As stated before, the axion source studied in this search is the M1 transition produced by thermal excitation of ^{57}Fe in the solar core. The isotope ^{57}Fe is stable and has 2.12% natural abundance, yielding an average ^{57}Fe density in the Sun's core of $(9.0 \pm 1.2) \times 10^{19} \text{ cm}^{-3}$. The uncertainty is mostly due to the different metal diffusion models in the core and is computed in Ref. [12]. The first excited state is at 14.4 keV, low enough to be thermally excited in the interior of the sun, which has an average temperature $kT \approx 1.3$ keV [13][14]. In this paper, we rely on Ref. [14] for the determination of the expected axion flux. The 15% error in the knowledge of ^{57}Fe density is taken into account. The error in the ^{57}Fe density was taken to be the error in the flux.

The Lagrangian that couples axions to nucleons is:

$$\mathcal{L} = a \bar{\psi}_i \gamma_5 (g_{AN}^0 \beta + g_{AN}^3 \tau_3) \psi. \quad (2.1)$$

Here, g_{AN}^0 and g_{AN}^3 are the iso-scalar and iso-vector coupling constants, model dependent, and τ_3 is a Pauli matrix.

To compute the expected axion flux, the axion-to-photon branching ratio for the decay of the 1st excited state of ^{57}Fe has to be taken into account [14, 15]:

$$\frac{\Gamma_a}{\Gamma_\gamma} = \left(\frac{k_a}{k_\gamma} \right)^3 \frac{1}{2\pi\alpha} \frac{1}{1+\delta^2} \left[\frac{g_{AN}^0 \beta + g_{AN}^3}{(\mu_0 - 1/2)\beta + \mu_3 - \eta} \right]^2 \quad (2.2)$$

where $\mu_0 = 0.88$ and $\mu_3 = 4.71$ are the isoscalar and isovector nuclear magnetic moments (in nuclear magnetons), δ is the E2/M1 mixing ratio for the nuclear transition, β and η are

64 nuclear structure dependent ratios. For the 14.4 keV de-excitation process their values are δ
 65 $= 0.002$, $\beta = -1.19$ and $\eta = 0.8$ [14]. With these values in Eq. (2.2), we have

$$\frac{\Gamma_a}{\Gamma_\gamma} = \left(\frac{k_a}{k_\gamma}\right)^3 1.82(-1.19g_{AN}^0 + g_{AN}^3) \quad (2.3)$$

66 for an axion with a total energy of 14.4 keV. The resulting axion flux, given by [16], will
 67 be:

$$\Phi_a = \left(\frac{k_a}{k_\gamma}\right)^3 \times 4.56 \times 10^{23} (g_{AN}^{eff})^2 \text{ cm}^{-2}\text{s}^{-1} \quad (2.4)$$

68 in which the prefactor has not been approximated to 1 to account for the non-relativistic
 69 limit and where $g_{AN}^{eff} \equiv (-1.19g_{AN}^0 + g_{AN}^3)$.

70 It is possible to evaluate the axion flux for specific models. In particular, in hadronic
 71 axions the axion-nucleon coupling constants are defined by the expressions [14, 15, 17]:

$$\begin{aligned} g_{AN}^0 &= -7.8 \times 10^{-8} \left(\frac{6.2 \times 10^6 \text{ GeV}}{f_A}\right) \left(\frac{3F - D + 2S}{3}\right) \\ g_{AN}^3 &= -7.8 \times 10^{-8} \left(\frac{6.2 \times 10^6 \text{ GeV}}{f_A}\right) \left((D + F)\frac{1 - z}{1 + z}\right) \end{aligned} \quad (2.5)$$

72 where $F \approx 0.48$ and $D = 0.77$ are invariant matrix elements of the axial current[15]. The
 73 Spin-Muon Collaboration gives the range for the flavor-singlet axial vector matrix element S
 74 of $0.15 \leq S \leq 0.50$ at 95% C.L [18] while Altarelli *et. al* give the range $0.37 \leq S \leq 0.53$ [19].
 75 For future considerations, we will consider the overlapping range $0.35 - 0.55$ for S .

76 It has to be underlined that values for g_{AN}^0 and for g_{AN}^3 in the DFSZ model depend
 77 on two additional unknown parameters, X_u and X_d , the so-called Peccei-Quinn charges of
 78 the u and d quark respectively [17]. These charges have positive-definite values constrained
 79 by the relation $X_u + X_d = 1$. The fluxes in the DFSZ model lie within an interval whose
 80 lower and upper bounds are determined not only by the range assumed for S , but also on the
 81 different possible combinations of X_d and X_u values. The axion-nucleon coupling constants
 82 are defined in this case by the expressions [17]:

$$\begin{aligned} g_{AN}^0 &= 5.2 \times 10^{-8} \left(\frac{6.2 \times 10^6 \text{ GeV}}{f_A}\right) \left(\frac{(3F - D)(X_u - X_d - 3)}{6} + \frac{S(X_u + 2X_d - 3)}{3}\right) \\ g_{AN}^3 &= 5.2 \times 10^{-8} \left(\frac{6.2 \times 10^6 \text{ GeV}}{f_A}\right) \frac{D + F}{2} \left(X_u - X_d - 3\frac{1 - z}{1 + z}\right). \end{aligned} \quad (2.6)$$

83 The fluxes of the 14.4 keV ^{57}Fe solar axions have the same order of magnitude in the
 84 KSVZ and in the DFSZ model, as can be seen in Figure 1. For a quantitative discussion of
 85 the data collected in the experiment here described, in the future we will assume $S = 0.5$
 86 and $X_d = 1$ (and consequently $X_u = 0$).

87 3 Axion interaction with matter: the axio-electric effect

88 The detection mechanism used in the present work is the axio-electric effect, which is the
 89 equivalent of a photo-electric effect with the absorption of an axion instead of a photon:
 90 $A + e + Z \rightarrow e + Z$.

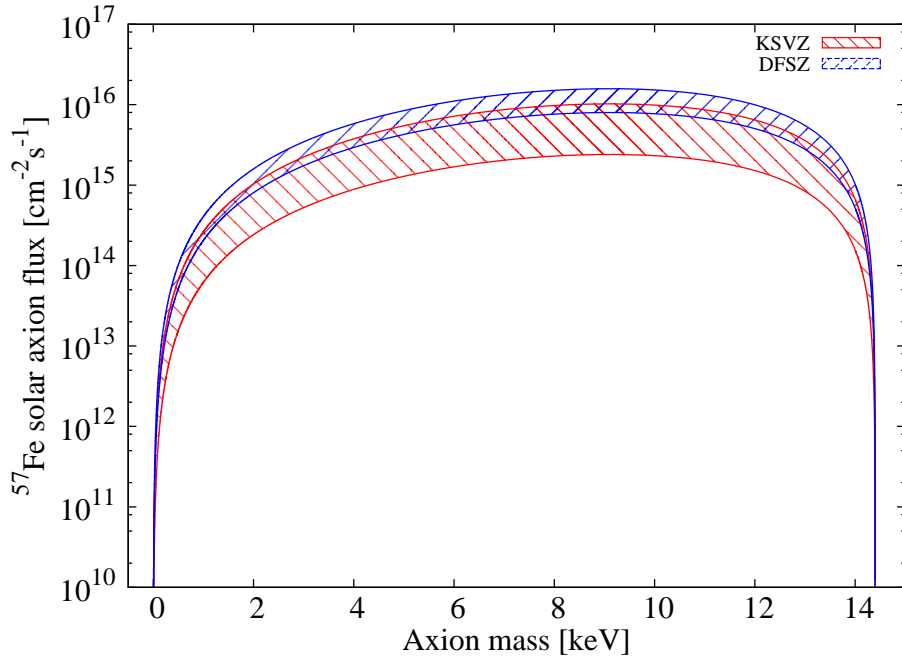


Figure 1. Expected fluxes of ^{57}Fe solar axions as a function of the axion mass. The lower/red and the upper/blue regions (partially overlapping) refer to the KSVZ and DFSZ models respectively. The bands correspond to the ranges spanned by the parameters S, X_d and X_u .

91 The purpose of this paper is to study ^{57}Fe solar axions both in the relativistic and
 92 non-relativistic realms, with masses in the latter case approaching the 14.4 keV energy of
 93 the ^{57}Fe first excited state. It is very convenient therefore to choose an expression for the
 94 axio-electric cross section σ_{Ae} which holds both in the extreme relativistic limit and for very
 95 cold axions, but is also capable of correctly describing the intermediate cases as well. Below
 96 we outline how this choice is made.

97 The two cross-section limits for $\beta \rightarrow 0$ and $\beta \rightarrow 1$, where β is the axion velocity, have
 98 been computed by M. Pospelov et al. (see for example Ref. [20]) in terms of f_A , and shown
 99 to be:

$$\begin{aligned} \sigma_{Ae} \Big|_{\beta \rightarrow 0} &\simeq \sigma_{pe}(m_A) \frac{3m_A^2}{4\pi\alpha f_A^2 \beta} \\ \sigma_{Ae} \Big|_{\beta \rightarrow 1} &\simeq \sigma_{pe}(E) \frac{E^2}{2\pi\alpha f_A^2}, \end{aligned} \tag{3.1}$$

100 where σ_{pe} is the photoelectric cross section, α the fine structure constant, E the axion
 101 energy and m_A the axion mass.

102 We intend, however, to express the cross sections more generally in terms of a dimen-
 103 sionless coupling constant g_{Ae} , defined by the interaction Lagrangian

$$\mathcal{L}_{int} = ig_{Ae} \bar{\psi} \gamma_5 \psi a \tag{3.2}$$

104 which couples the axion field a to the electron field ψ .

105 In order to do that, we recall that the formulae in Eq. (3.1) are obtained starting from
 106 the two equivalent forms [5] of the axion-electron interaction Lagrangian

$$\begin{aligned}\mathcal{L}_{int1} &= -\frac{\partial_\mu a}{f_A} \bar{\psi} \gamma^\mu \gamma_5 \psi \\ \mathcal{L}_{int2} &= i \frac{2m_e}{f_A} \bar{\psi} \gamma_5 \psi a .\end{aligned}\tag{3.3}$$

107 The comparison between Eq. (3.2) and the second expression in Eq. (3.3) shows that
 108 the two limiting forms for the axio-electric cross section in terms of g_{Ae} can be achieved by
 109 replacing $f_A = 2m_e/g_{Ae}$ in Eq. (3.1), obtaining:

$$\begin{aligned}\sigma_{Ae} \Big|_{\beta \rightarrow 0} &\simeq g_{Ae}^2 \sigma_{pe}(m_A) \frac{3m_A^2}{16\pi\alpha\beta} \\ \sigma_{Ae} \Big|_{\beta \rightarrow 1} &\simeq g_{Ae}^2 \sigma_{pe}(E) \frac{E^2}{8\pi\alpha} .\end{aligned}\tag{3.4}$$

110 A convenient general formula which reduces to the asymptotic expressions of Eq. (3.4)
 111 has been proposed in Ref. [21, 22] and adopted also in Ref. [23]. In the following analysis,
 112 we will use a similar expression, given by

$$\sigma_{Ae}(E) = \sigma_{pe}(E) \frac{g_{Ae}^2}{\beta} \frac{3E^2}{16\pi\alpha m_e^2} \left(1 - \frac{\beta^{\frac{2}{3}}}{3} \right) ,\tag{3.5}$$

113 which differs from the aforementioned formula – reported in Ref. [21–23] – as the expo-
 114 nent β is $2/3$ instead of unity as in the quoted papers. We have introduced this change since,
 115 as suggested by M. Pospelov [24], the modified formula in Eq. (3.5) describes with better
 116 accuracy the cross section over the full β range.

117 In specific axion models, the dimensionless constant g_{Ae} is related to the electron mass
 118 and f_A so that

$$g_{Ae} = C_e m_e / f_A ,\tag{3.6}$$

119 where C_e is a model-dependent parameter that is of the order unity when the coupling
 120 to electrons occurs at the tree level. We have already seen that $C_e = 2$ in the approach
 121 followed by M. Pospelov et al. [20].

122 In the DFSZ axion models, where the coupling at the tree level occurs, the parameter
 123 C_e is usually expressed as

$$C_e = \frac{1}{3} \cos^2(\beta_{DFSZ}) ,\tag{3.7}$$

124 where $\tan(\beta_{DFSZ})$ is the ratio of two Higgs vacuum expectation values. We will take
 125 $C_e = \frac{1}{3}$, which is equivalent to take $X_d = 1$, where X_d is the Peccei-Quinn charge of the d
 126 quark introduced before. Therefore, g_{Ae} is numerically given by

$$g_{Ae} \simeq 1.68 \times 10^{-4} / f_A [\text{GeV}] \simeq 2.84 \times 10^{-8} m_A [\text{keV}].\tag{3.8}$$

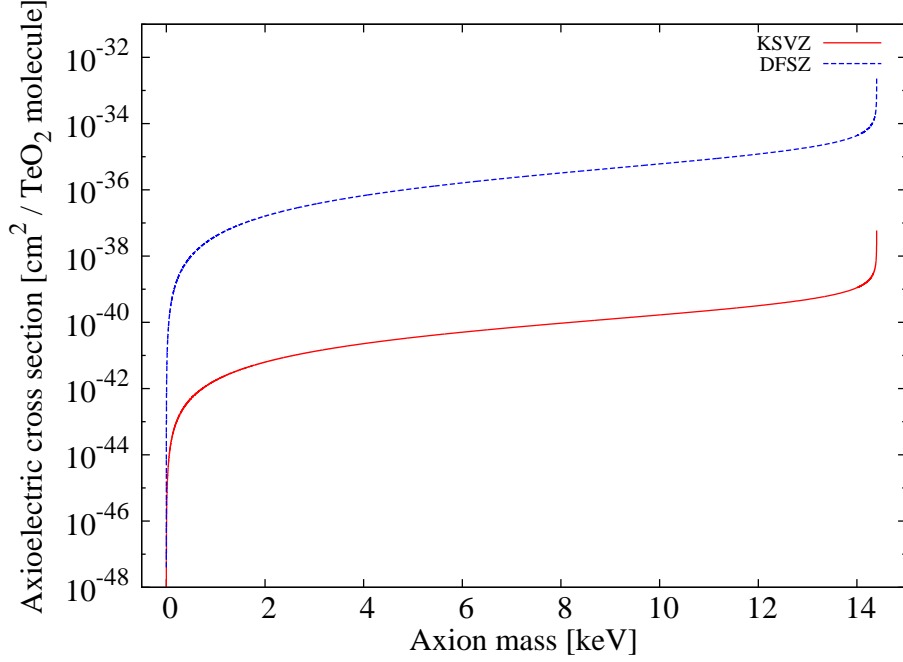


Figure 2. Cross sections on TeO_2 of 14.4 keV axions for axioelectric effect as a function of the axion mass in the case of KSVZ model (lower/red curve) and DFSZ model (upper/blue curve).

127 In the KSVZ axion model there is no tree-level couplings to electron, so g_{Ae} is much
 128 smaller (by a factor of about α^2), being determined only by radiative corrections [25]:

$$g_{Ae} = \frac{3\alpha^2 N m_e}{2\pi f_A} \left(\frac{E}{N} \ln \frac{f_A}{m_e} - \frac{24 + z + w}{31 + z + w} \ln \frac{\Lambda}{m_e} \right), \quad (3.9)$$

129 where $E/N = 8/3$ in GUT models with $N = 3$ (number of generations), and $\Lambda \approx 1$ GeV is
 130 the QCD cutoff scale. The factor containing z and w arises from the axion-pion mixing and
 131 is cut off at the QCD confinement scale. In this case, g_{Ae} is numerically given by

$$g_{Ae} \simeq \frac{3.9 \times 10^{-8}}{f_A[\text{GeV}]} \left(2.67 \times \ln \frac{f_A}{m_e} - 14.65 \right). \quad (3.10)$$

132 We have computed the cross sections foreseen by the two models in the case of a TeO_2
 133 target and at the axion total energy of 14.4 keV. For the photoelectric cross section on a TeO_2
 134 molecule at 14.4 keV we have taken the value $1.17 \times 10^{-20} \text{ cm}^2$ [26]. The two cross sections
 135 are compared in Figure 2, where the ratio of the order of α^2 between the KSVZ and DFSZ
 136 estimations is appreciable.

137 4 Experiment

138 In the analysis shown in the present work we will focus on the results from a specific R&D
 139 run dedicated to the CUORE experiment.

140 CUORE will be an array of 988 TeO_2 crystals, each with size $5 \times 5 \times 5 \text{ cm}^3$ and weight
 141 750 grams, which will be operated as bolometers at a temperature of about 10 mK to search

142 for the neutrinoless double beta decay of ^{130}Te and other rare events. A description of the
143 CUORE technique and the basic principles behind bolometers is given in [27], [28], [29], and
144 [30].

145 The crystals to be used for CUORE are produced using special procedures developed to
146 minimize radioactive contaminants [31] at the Shanghai Institute for Ceramics of the Chinese
147 Academy of Science (SICCAS), and are shipped in batches to the Laboratori Nazionali del
148 Gran Sasso (LNGS) located in Assergi, Italy. Four crystals are taken at random from each
149 batch to measure their radioactive contamination levels and evaluate their performance as
150 bolometers at low temperature. Each one of these runs is called a Cuore Crystal Validation
151 Run, or CCVR [32]. This paper will present the analysis data from the second run, known
152 as CCVR2.

153 The four TeO_2 crystals (labeled B1,B2,B3,B4), have a total active mass of 3 kg and are
154 mounted in a specially designed copper frame which is placed inside a dilution refrigerator
155 at LNGS. The cryostat is maintained at a working temperature of approximately 8-10 mK
156 throughout the duration of the run.

157 Glued on each CCVR bolometer are two Neutron Transmutation Doped (NTD) ther-
158 mistors to read out the thermal signal [33]. For CCVR2, data were collected for a total of
159 19.4 days for a total exposure of 43.65 kg·d. Calibrations were performed in the middle and
160 end of the run with a ^{232}Th γ -ray source inserted inside the Pb shielding, close to the cryostat
161 outer vacuum vessel.

162 The CUORICINO experiment [27, 34], had bolometers whose typical threshold was 50
163 keV. Since the Q-value for ^{130}Te is at 2527 keV [35–37], a threshold at 50 keV was more
164 than satisfactory for $\beta\beta$ -decay searches. However, to investigate physical events at lower
165 energies, new procedures were needed to lower the energy threshold. For this reason a special
166 low-energy trigger was developed and applied offline, exploiting the fact that the standard
167 CUORE DAQ used in the CCVR runs collects data continuously and with no hardware
168 trigger using 125 Hz 18-bits digitizers. This trigger algorithm maximizes the signal to noise
169 ratio by filtering the data with a known power spectrum and a reference signal shape. On
170 each of the four bolometers, we selected the thermistor in which the trigger reached the lowest
171 energy threshold. The thresholds were 10 keV for B1, 3 keV for B2 and 2.5 keV for B3 and
172 B4. For the present work we chose to include only the bolometers whose thresholds were
173 lower than 4 keV as to include the peak at 4.7 keV. Although the physical interpretation of
174 this line is unclear, the peak appeared to be constant in time [39] and therefore we used to
175 monitor the stability of the cuts. The efficiencies were 0.91 ± 0.10 for B2 and 0.83 ± 0.09
176 for B3 and B4. We took the statistical fluctuation of the 4.7 keV peak rate in the energy
177 spectrum as the systematic uncertainty of the efficiency. A full description of the trigger and
178 its performance is given in [38, 39].

179 Energy calibration in this very low energy region is not done with the ^{232}Th γ -ray lines,
180 which are normally used for higher energy calibration. The energy region between 2.5 and
181 300 keV is calibrated with a third order polynomial fit using a set of x-ray and γ -ray lines
182 from metastable Te states that result from cosmogenic activation. The crystals spend several
183 weeks above ground while they are being shipped by sea¹ between the production site in
184 Shanghai, China and arrival at the underground storage site at LNGS. The main γ -ray lines
185 used in the calibration for present work are reported in Table 1. As a further check, the
186 bolometers were irradiated with a ^{55}Fe source deposited on the copper holder. The x-rays

¹The shipment of two (out of four) crystals was actually made by airplane, which induces a slightly higher activation.

Energy [keV]	Source	Life-Time (days)
30.4912	Sb x-ray	–
88.26 ± 0.08	^{127m}Te	109 ± 2
105.50 ± 0.05	^{129m}Te	33.6 ± 0.1
144.78 ± 0.03	^{125m}Te	57.40 ± 0.15
247.5 ± 0.2	^{123m}Te	119.7 ± 0.1
293.98 ± 0.04	^{121m}Te	154 ± 7

Table 1. List of γ -ray lines from meta-stable Te isotopes used in this analysis for the energy calibration in the energy region between 2.5 and 300 keV. The lines are available from cosmogenic activation of Te during shipment, and have half-lives spanning from 33.6 days and 119.7 days.

187 produced, with nominal energy between 5.888 and 6.490 keV, were shifted by only $+(48\pm 16)$
188 eV [39].

189 5 Results

190 In order to reject thermal and microphonic noise, the pulses are selected using the shape
191 indicator variable described in [38]. This variable is based on the χ^2 of the fit of the waveforms
192 with the expected shape of the signal. Event selection is made by means of a scatter plot in
193 which the two types of pulses form different bands. The determination of the pulse shape
194 cut efficiencies, described in detail elsewhere [39] have been evaluated on the 4.7 keV peak
195 and are equal to 1. They were found to be almost completely energy independent for events
196 above 3 keV.

197 The low energy spectrum, below 40 keV, is shown in Fig. 3. It is modeled with two
198 exponentials, one for the region lower than 5 keV, one for the background above 7 keV, and
199 two Gaussians to model the peaks around 4.7 and 30.5 keV. All parameters are free in the
200 fit. From the fit to the spectrum in Figure 3 we obtained consistent results for the two
201 Gaussian widths: $\sigma_{4.7} = 0.29 \pm 0.02$ keV and $\sigma_{30.5} = 0.33 \pm 0.03$ keV. This was expected
202 since at low energies the resolution of the bolometers is not dominated by signal fluctuations
203 and we know that the energy dependence is weak. A fit in the region 11-18 keV (inset of
204 Figure 3) is applied to extract limits on the axion detection rate. We used an exponential
205 function to model the continuum background and a Gaussian centered at 14.4 keV for the
206 axion peak. The width of the Gaussian is fixed to the weighted average of the 4.7 and 30.5
207 keV resolutions $\sigma_{14.4} = 0.31$ keV. The best fit for the axion rate yields -0.1 ± 0.3 c·kg⁻¹·d⁻¹.
208 This is consistent with zero and the upper limit is set integrating the posterior p.d.f after
209 marginalization over systematics uncertainties and with a flat prior on the rate in the physical
210 region. Systematics consist of a 15% uncertainties on efficiencies and ⁵⁷Fe content in the solar
211 core and are taken to be Gaussian. The resulting 95% confidence level upper limit for the
212 axion detection rate is 0.58 c·kg⁻¹·d⁻¹.

213 6 Limits on the axion-relevant parameters

214 Using the results described in the previous Section, it is possible to set excluded regions for
215 the coupling involved in this search, i.e. g_{Ae} and $g_{AN}^{eff} \equiv g_{AN}^0\beta + g_{AN}^3$. In the framework of
216 specific models, we can also set limits on the axion mass m_A or equivalently on the symmetry-
217 breaking energy scale f_A .

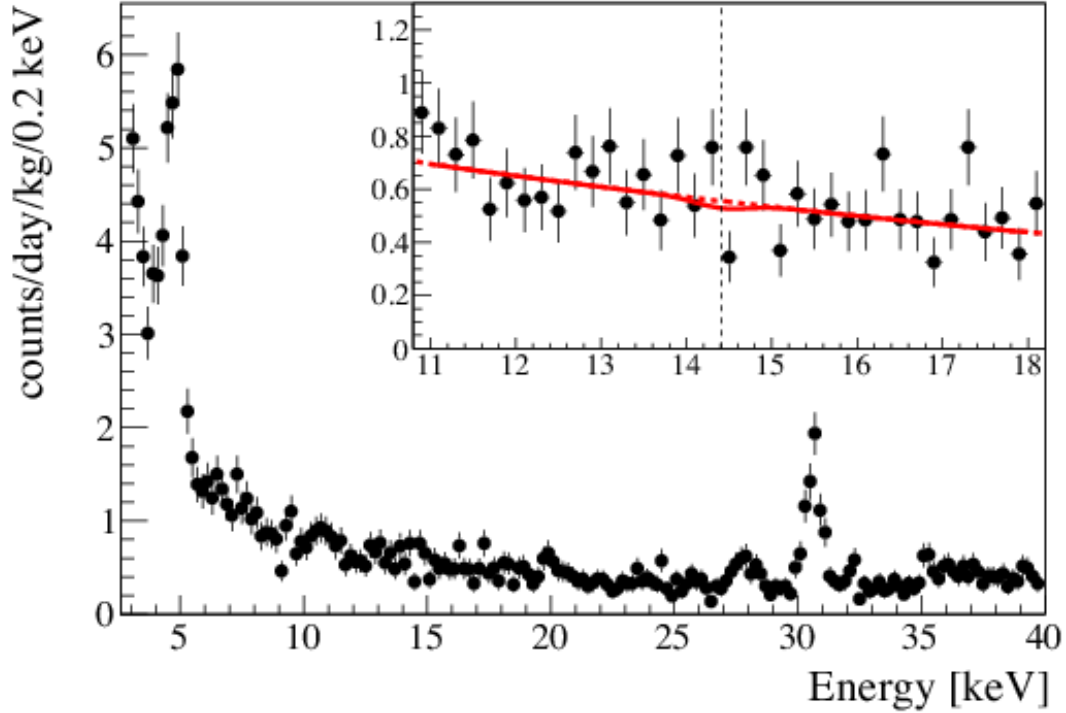


Figure 3. Energy spectrum for the low energy region between threshold and 40 keV. The two peaks at 4.7 keV and 30.49 keV are those used to study the energy resolution at low energy. The axion region around 14.4 keV is magnified in the inset with the fit result shown as red curve. No peak is observed at 14.4 keV, the M1 transition energy of ^{57}Fe for solar axions.

218 Three scenarios will be considered:

- 219 1. g_{Ae} and g_{AN} are completely model independent and the dependency on the axion mass
220 comes only from kinematical factors (see Sections 2.4 and 3.5).
- 221 2. g_{Ae} is a model independent parameter while g_{AN}^{eff} is evaluated in the framework of
222 the DFSZ and KSVZ models, using the considerations and the expressions reported in
223 Section 2.
- 224 3. both g_{Ae} and g_{AN}^{eff} are evaluated in the framework of the DFSZ and KSVZ models,
225 bringing in our knowledge of the axioelectric effect summarized in Section 3.

226 Using the relationships given in (2.4) and (3.5), it is possible to obtain the upper limits
227 for $(g_{AN}^{eff}) \times g_{Ae}$ as a function of the axion mass m_A . Fig. 4 shows this model independent
228 limit.

229 In the second approach, the allowed range of g_{Ae} can be calculated as a function of
230 the axion mass m_A , assuming the values predicted by the DFSZ and KSVZ models for the
231 combination of g_{AN}^0 and g_{AN}^3 present in the branching ratio expression for the axion emission
232 from the excited state of ^{57}Fe . The curves reported in the plot assume $S = 0.5$ for the
233 flavor-singlet axial vector matrix element in both models, while the Peccei-Quinn charge of

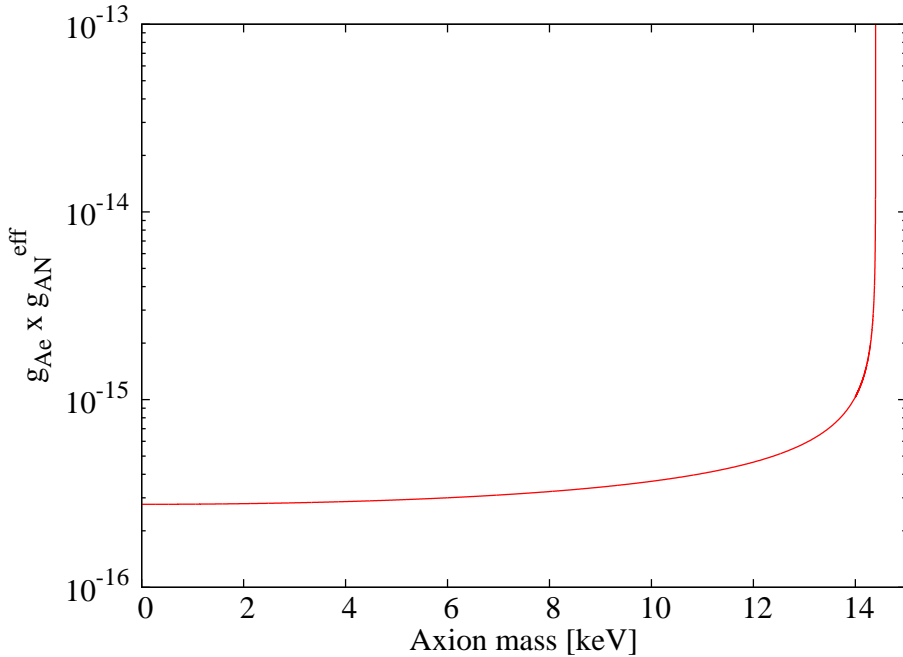


Figure 4. Upper limits for $g_{Ae} \times g_{AN}^{eff}$ as a function of the axion mass m_A obtained using the TeO_2 data.

234 the d quark X_d is set equal to 1 for the DFSZ model. This is the value that maximizes the
 235 DFSZ axioelectric cross section that will be used to set a limit on the axion mass. Figure 5
 236 shows the restricted ranges for g_{Ae} .

237 Finally, we have considered the relationships between the axioelectric cross sections
 238 and the axion mass in the DFSZ model with $X_d = 1$ and in the KSVZ model, and we
 239 have compared them with our bounds (see again Figure 5). This allows to set limits on the
 240 axion masses, which correspond to 19.2 eV and 250 eV at 95% c.l. in the DFSZ and KSVZ
 241 models respectively assuming $S = 0.5$ in both cases. In terms of the symmetry-breaking
 242 energy scale f_A , these limits correspond to lower bounds of 3.12×10^5 GeV (DFSZ model)
 243 and 2.41×10^4 GeV (KSVZ model). The corresponding solar axion fluxes are $\sim 1.2 \times 10^{11}$
 244 $\text{cm}^{-2}\text{s}^{-1}$ and $\sim 1.2 \times 10^{13}$ $\text{cm}^{-2}\text{s}^{-1}$. If we consider a range $[0.35, 0.55]$ for S (as discussed in
 245 Section 2), the limits on the masses are in the ranges $[18.2, 19.5]$ eV in the DFSZ model and
 246 $[232, 339]$ eV in the KSVZ model.

247 Our results can be placed in a global context by comparing in a $g_{Ae} - m_A$ plane our
 248 bounds with those achieved by other searches, which use a variety of approaches and tech-
 249 niques. This comparison is shown in Fig. 6, from which one can appreciate that our results
 250 are at the level of the most competitive searches in this field.

251 7 Summary and Conclusions

252 An experimental search for axions emitted from the first excited state of ^{57}Fe in the solar
 253 core was performed. The calculation of the axion flux was made both in the framework of
 254 the DFSZ and KSVZ models. The detection technique employed a search for a peak in the
 255 energy spectrum at 14.4 keV when the axion is absorbed by an electron via the axio-electric

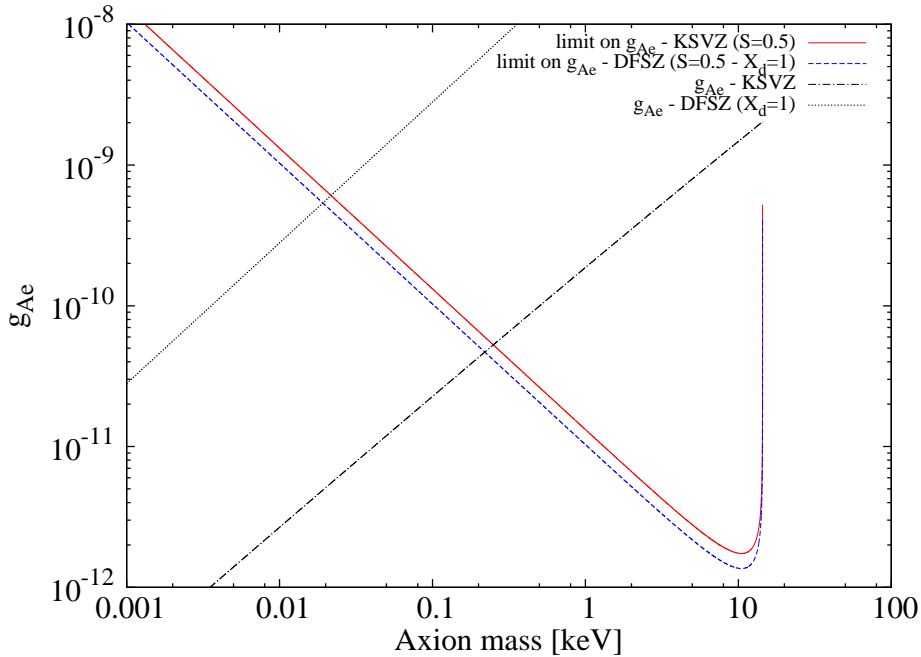


Figure 5. Upper limits on g_{Ae} obtained using the TeO_2 results, assuming axion emission from the excited state of ^{57}Fe in the in the KSVZ model (solid/red line) and in the DFSZ model (dashed/blue line), with $S = 0.5$ and $X_d = 1$ (see text). The inclined lines represent the relationships between the axioelectric cross sections and the axion mass in the KSVZ model (dashed-dotted line) and in the DFSZ model with $X_d = 1$ (dotted line). The abscissae of the points where our bounds and the axioelectric predictions cross provide the limits on the axion mass (and consequently on the symmetry-breaking scale) in the two models (see text for these limits).

256 effect. The cross section for this process is assumed to be proportional to the photo-electric
 257 absorption cross section of photons by electrons and is evaluated in the DFSZ and KSVZ
 258 axion models. In this experiment 43.65 kg·d of data were analyzed resulting in a lower bound
 259 on the Peccei-Quinn energy scale of 3.12×10^5 GeV (DFSZ model) and 2.41×10^4 GeV (KSVZ
 260 model), for a value for the flavor-singlet axial vector matrix element of $S = 0.5$.

261 The CUORE experiment will have about 740 kg TeO_2 . With an anticipated live-time
 262 of 5 years the exposure will be 1.4×10^6 kg·d. With a similar background as the one reported
 263 here the expected bound on f_A will be increased by approximately an order of magnitude.

264 8 Acknowledgments

265 The CUORE Collaboration thanks the Directors and Staff of the Laboratori Nazionali del
 266 Gran Sasso and the technical staffs of our Laboratories. This work was supported by the
 267 Istituto Nazionale di Fisica Nucleare (INFN); the Director, Office of Science, of the U.S. De-
 268 partment of Energy under Contract Nos. DE-AC02-05CH11231 and DE-AC52-07NA27344;
 269 the DOE Office of Nuclear Physics under Contract Nos. DE-FG02-08ER41551 and DE-
 270 FG03-00ER41138; the National Science Foundation under Grant Nos. NSF-PHY-0605119,
 271 NSF-PHY-0500337, NSF-PHY-0855314, and NSF-PHY-0902171; the Alfred P. Sloan Foun-
 272 dation; and the University of Wisconsin Foundation. We also warmly thank C. Peña-Garay,
 273 A. Serenelli and F. Villante for useful discussion about solar core ^{57}Fe content.

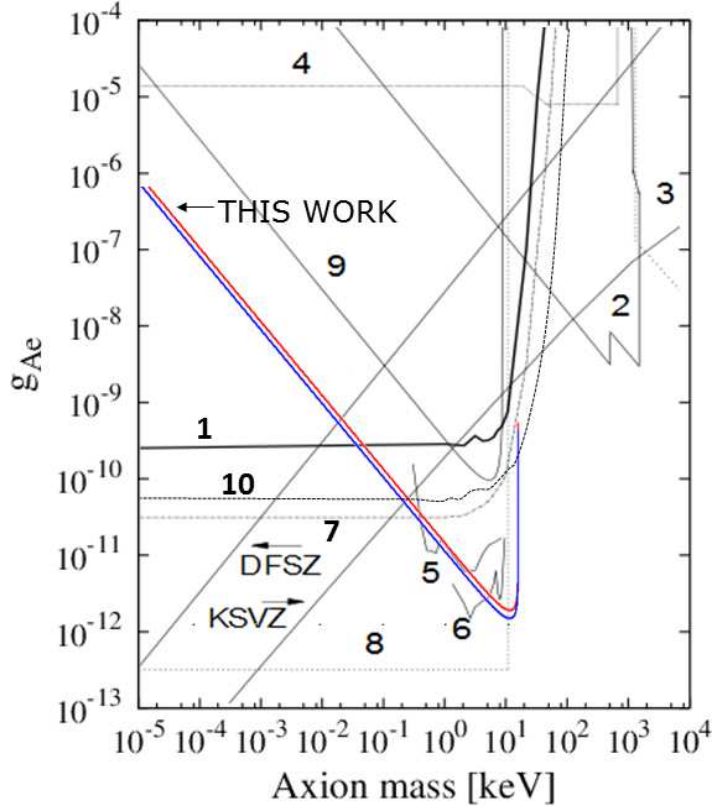


Figure 6. Bounds on g_{Ae} obtained in this work (and already reported in Fig. 5) are given by the upper (red) line and lower (blue) line for the KSVZ and DFSZ model respectively for the production of solar axions. These bounds are compared with (1) search for solar axions produced by Compton and bremsstrahlung processes with a Si(Li) detector [22], (2) reactor experiments and solar axions with energy of 0.478 and 5.5 MeV [40–44], (3) beam dump experiment [45, 46], (4) decay of orthopositronium [47], (5) CoGeNT [48], (6) CDMS [49], (7) bound for the axion luminosity of the sun [50], (8) red giants [51], (9) experiment with ^{169}Tm [52] and (10) XMASS [53]. The inclined curves represent the relationships between g_{Ae} and m_A in the DFSZ and KSVZ models. The figure is adapted from Ref. [22].

274 References

- 275 [1] C. A. Baker et al., Phys. Rev. Lett. **97** no. 13, 131801 (2006).
 276 [2] R. D. Peccei and Helen R. Quinn, Phys. Rev. D **16** no. 6, 17911797 (1977).
 277 [3] S. Weinberg, Phys. Rev. Lett. **40**, 223 (1978).
 278 [4] F. Wilczek, Phys. Rev. Lett. **40**, 279 (1978).
 279 [5] G.G. Raffelt, J. Phys A: Math. Theor. **40**, 6607 (2007).
 280 [6] C. Hagmann et al in C. Amsler et al, (particle Data Group) Phys Lett. **B667**,1 (2008).
 281 [7] Jihn Kim and Gianpaolo Carosi, Rev. Mod. Phys. **82**, 587 (2010).
 282 [8] P. Sikivie and Q. Yang, Phys. Rev. Lett. **103**, 111301 (2009).
 283 [9] A. R. Zhitniskiy, Yad. Fiz. **31**, 497 (1980); M. Dine et al., Phys. Lett. B **104**, 199 (1981).
 284 [10] J. E. Kim, Phys. Lett. **43**, 103 (1979); M. A. Shifman et al., Nucl. Phys. B **166**, 493 (1980).

- 285 [11] B. Beltran et al. (CAST Collaboration), PoS **HEP2005** 022 (2006) [arxiv: hep-ex/0507007].
- 286 [12] A.Serenelli et al., *Astrophys. J.* **705** L123-L127 (2009).
- 287 [13] S. Moriyama, *Phys. Rev. Lett.* **75** no. 18, 3222-3225 (1995).
- 288 [14] W. C. Haxton and K. Y. Lee, *Phys. Rev. Lett.* **66** no. 20, 2557-2560 (1991).
- 289 [15] F. T. Avignone, *Phys. Rev. D* **37** 618 (1988).
- 290 [16] S. Andriamonje et al. (CAST collaboration), *JCAP12* **002** (2009).
- 291 [17] D. B. Kaplan, *Nucl. Phys. B* **260** , 215-226 (1985).
- 292 [18] D. Adams et al. (Spin Muon Collaboration), *Phys. Rev. D* **56** no. 9, 5330-5358 (1997).
- 293 [19] G. Altarelli et al., *Nucl. Phys. B* **496** no. 1-2, 337-357 (1997).
- 294 [20] M. Pospelov et al., *Phys. Rev. D* **78**, 115012 (2008).
- 295 [21] A. Derevianko et al., *Phys. Rev. D* **82**, 065006 (2010).
- 296 [22] A. V. Derbin et al., *JETP Lett.* **92**, 379 (2012).
- 297 [23] K. Arisaka et al., arXiv 1209.3810v4.
- 298 [24] M. Pospelov, private communication.
- 299 [25] M. Srednicki, *Nucl. Phys. B* **260** , 689-700 (1985).
- 300 [26] <http://physics.nist.gov/PhysRefData/Xcom/html/xcom1.html>
- 301 [27] E. Andreotti et al. (CUORICINO Collaboration), *Phys. Rev. C* **85** 045503 (2012).
- 302 [28] E Andreotti et al. (CUORICINO Collaboration), *Astrop. Phys.* **34** 822-831 (2011).
- 303 [29] C. Arnaboldi et al. (CUORICINO Collaboration), *Phys.Rev. C* **78** 035502 (2008).
- 304 [30] F. Alessandria et al. (CUORE Collaboration), [arxiv:hep-ex/1109.0494].
- 305 [31] C. Arnaboldi et al., *Journ. of Crys. Growth*, vol. **312**, p. 2999-3008 (2010).
- 306 [32] F. Alessandria et al. [arXiv:nucl-ex/1108.4757]
- 307 [33] E. Haller, *J. App. Phys.* **77**, 2857 (1995).
- 308 [34] E. Andreotti et al. (CUORICINO Collaboration), *Astrop. Phys.* **34** 643-648 (2011).
- 309 [35] M. Redshaw et al., *Phys. Rev. Lett.* **102** 212-502 (2009).
- 310 [36] N.D. Scielzo et al., *Phys. Rev.* **C80** 025501 (2009).
- 311 [37] S. Rahaman et al., *Phys. Lett.* **B 703** 412 (2011).
- 312 [38] S. Di Domizio, F. Orto, and M. Vignati, *JINST* **6** P02007 (2011).
- 313 [39] F. Alessandria et al., *JCAP01* **038** (2013).
- 314 [40] M.Altmann, Y. Declais, F. v. Feilitzsch, et al., *Z. Phys.C* **68**, 221 (1995).
- 315 [41] H. M. Chang et al. (Texono Collab.), *Phys. Rev. D* **75**,052004 (2007).
- 316 [42] G. Bellini et al. (Borexino Collaboration) *Eur. Phys. J. C* **54**, 61-72 (2008).
- 317 [43] G. Bellini et al. (Borexino Collaboration) *Phys. Rev D* **85**, 092003 (2012).
- 318 [44] A. V. Derbin, A. S. Kayunov, and V.N. Muratova, *Bull. Russ. Acad. Sci.: Phys.* **74**, 805 (2010).
- 319 [45] A. Konaka, K. Imai, H. Kobayashi, et al., *Phys. Rev.Lett.* **57**, 659(1986).
- 320 [46] J. D. Bjorken, S. Ecklund, W. R. Nelson, et al., *Phys.Rev. D* **38**, 3375 (1988).
- 321 [47] S. Asai, S. Orito, K. Yoshimura, and T. Haga, *Phys. Rev.Lett.* **66**, 2440 (1991).
- 322 [48] C. E. Aalseth et al. (CoGeNT Collab.), *Phys. Rev. Lett.* **101**, 251301 (2008).

- 323 [49] Z. Ahmed et al. (CDMS Collab.), Phys. Rev. Lett. 103, 141802 (2009).
324 [50] P. Gondolo and G. G. Raffelt, Phys. Rev. D 79, 107301(2009).
325 [51] G. G. Raffelt, Lect. Notes Phys. 741, 51 (2008).
326 [52] A. V. Derbin, A. S. Kayunov, V. N. Muratova, D.A. Semenov, E.V. Unzhakov, Phys. Rev. D
327 83, 023505 (2011).
328 [53] K. Abe, K. Hieda, K. Hiraide, S. Hirano, Y. Kishimoto, K. Kobayashi, S. Moriyama and
329 K. Nakagawa et al., arXiv:1212.6153v2 [astro-ph.CO].